Available online at www.sciencedirect.com
ScienceDirect
Remote Sensing of Environment 111 (2007) 228–241
Remote Sensing of Environment
www.elsevier.com/locate/rse

The semi-analytical snow retrieval algorithm and its application to MODIS data

M. Tedesco [a,b,*], A.A. Kokhanovsky [c]

[a] University of Maryland, Baltimore County - GEST, Baltimore, MD, USA
[b] NASA Goddard Space Flight Center, Greenbelt, MD, USA
[c] Institute of Environmental Physics, University of Bremen, O. Hahn Allee 1, D-28334, Bremen, Germany

Received 22 July 2006; received in revised form 7 February 2007; accepted 10 February 2007

Abstract

Grain size is a key parameter of a snowpack, affecting its thermodynamic state and influencing the spectral snow albedo. Differently from visible wavelengths, where the sensitivity to grain size is very low, in the near-infrared band there is a strong sensitivity of the reflectance to the grain size. This sensitivity provides the basis for the retrieval of grain size. In this paper we introduce a new snow retrieval algorithm that makes use of near-infrared measurements in which snow is modeled as a semi-infinite, weakly absorbing medium. It is assumed that the dense packing effects can be neglected and the radiative transport in snow can be studied using the standard radiative transfer equation extensively used, e.g., in cloud optics. The shape of grains is accounted for in the framework of fractal snow grain model. The performance of the algorithm is evaluated using ground-based measurements of snow albedo and results from a different retrieval algorithm. The technique is applied to study the changes of snow properties before and just after snow fall as seen by two MODIS sensors on TERRA and AQUA satellites. These satellites fly approximately 3 h and half apart (10:30 a.m. and 1:30 p.m. equator crossing time). The values of grain size retrieved from MODIS are also compared with values of grain size collected on ground. However, the area observed by MODIS including the locations of ground measurements was completely covered by clouds on the date of the measurements and the comparison could be performed only for the two previous days. A sensitivity analysis of the retrieval error due to atmospheric correction is also performed. Results show that the error on grain size retrieval induced by atmospheric correction ranges between ±5% and ±40%, depending on the grain size.

Keywords: Grain size; MODIS; Snow retrieval

1. Introduction

Snow is a fundamental element of the global water and energy cycles. The estimation of snow properties and relative distribution provide useful information that can benefit several aspects of hydrological, climatological and meteorological fields. Part of the amount of water stored within the snowpack during the winter time provides fresh drinkable water to surrounding areas when snow melts; also, as snow is a highly reflecting natural medium covering a significant portion of the land, it also plays a crucial role in the Earth's radiation budget. For large scale mapping purposes, remote sensing by means of space-borne instruments represents a suitable tool. Within this framework, optical and infrared (IR) data can provide information on the near-surface layers of the snowpack at a high spatial resolution, although the temporal resolution is strongly limited by solar illumination and clouds presence.

Grain size is a key parameter for characterizing snowpack properties from several points of view. Indeed, grain size can be related to the thermodynamic state of a snowpack, as metamorphism of snow crystals is driven by gradients of temperature and vapor density within the snowpack. Therefore, mapping spatial and temporal trends of snow grain size can be useful for characterizing the thermal state of the snowpack and supporting the estimation of the timing and spatial distribution of snowmelt as well. Also spectral snow albedo is controlled strongly by grain size. In the visible region, the sensitivity of albedo to grain size is small because pure ice is transparent at

* Corresponding author. University of Maryland, Baltimore County - GEST, Baltimore, MD, USA.
E-mail address: mtedesco@umbc.edu (M. Tedesco).

0034-4257/$ - see front matter © 2007 Elsevier Inc. All rights reserved.
doi:10.1016/j.rse.2007.02.036

these wavelengths (e.g. the probability that a photon will be absorbed once it enters an ice grain is small and does not considerably increase with the grain size). At these wavelengths, the snow albedo and also its reflection function are sensitive to the presence of absorbing impurities. On the other hand, as pure ice is moderately absorptive in the near-infrared bands, the reflectance shows a stronger sensitivity to the grain size than in the visible. The greatest sensitivity is at 1.0–1.3 μm, with the reflectance increasing with illumination angle, especially for larger grains. This sensitivity furnishes the basis for the retrieval of grain size at these wavelengths. The dependence of the snow reflection function on the concentration of impurities in the near IR is low due to strong light absorption by ice crystals and relatively small absorption of light by impurities in snow (e.g., soot and dust) is hardly detectable in the near IR. Therefore, retrieving the grain size from the near IR, one can get the concentration of pollutants performing calculations for a retrieved grain size in the visible. The difference between the calculated and measured reflectance gives the concentration of pollutants as described by Kokhanovsky and Zege (2004).

Most of the models describing the relationships between albedo at visible/infrared wavelengths and snow grain size assume that ice grains are spherical particles. Here, the scattering of light by spherical particles can be described by Mie theory (Mie, 1908) with high accuracy. In reality, snow grains are irregularly shaped. Often, the combination of simple regular shapes with different weights are used to model absorption and scattering characteristics of ice grains (see, e.g., http://www.ssec.wisc.edu/~baum/Cirrus/IceCloudModels.html). An alternative approach is based on a stochastic single particle model in which the particle should have similar light scattering characteristics to the ensemble of irregularly shaped particles. In order, to model a stochastic particle it is possible to use a fractal-based approach, where the particle is modeled as a Koch fractal of the second generation (Macke et al., 1996; Kokhanovsky, 2006). A recent study proposes an approximate equation for the reflection function of a semi-infinite non-absorbing medium in which the particles are modeled according to this approach (Kokhanovsky, 2005). It must be emphasized that particles of complex shapes are characterized by very similar phase functions independently on the particular choice of the geometry of a stochastic particle (Kokhanovsky & Zege, 2004). Corresponding phase functions are featureless and almost constant in the backward hemisphere relevant for space remote sensing applications.

In this study we make use of the asymptotic equations of the radiative transfer theory developed under the assumptions of fractal particles for retrieving the dimension of grain ice from near-infrared measurements of reflectance. We apply the inversion procedure to both ground-based and satellite data. First we test the retrieval in the case of a controlled experiment when the atmospheric effects are negligible and the comparison with measurements of grain size values derived from observations and from image processing analysis of snow samples is performed. The values of grain size retrieved under the assumption of fractal particles are compared with those derived by assuming spherical particles and with those derived from an approach different from the one here proposed. Then, the inversion procedure is applied to space-borne data collected by the Moderate Resolution Imaging Spectroradiometer (MODIS) to provide maps of grain size. We make use of the product called MODIS Surface Reflectance gridded to 500 m resolution (e.g. Vermote & Vermeulen, 1999). MODIS Snow Cover Area (SCA) and geo-location products are also used in the analysis. These products are described in the following in more details. The values retrieved from satellite data are compared with values of grain size collected over a large area within the framework of the NASA Cold Land Processes Experiment (CLPX-1). Unfortunately, because of cloudy sky conditions, it was not possible to select a day where simultaneously ground – based and satellite measurements of the grain size are performed. The closest possible measurements are 24 h apart. This leads to differences in the ground-based and satellite-derived grain sizes. We also discuss other potential sources of discrepancies between satellite-retrieved and measured values.

The paper is structured as follows: in Section 2, we report a review of the works available in the literature to retrieve the grain size from optical measurements; in Section 3, the theoretical basis of the approach used here for the inversion and its equations are reported; in Section 4, we give the results of the retrieval approach using ground-based data and discuss the derived grain sizes obtained with and without fractal particles assumption; then, in Section 5, we report the results derived from MODIS data; in Section 6 we give a general discussion of the obtained results and dedicate Section 7 to the conclusion and future work.

2. Background

The retrieval of snow grain size from space is possible because snow reflection function primarily depends on the size of scatterers in the near-IR (Dozier & Schneider, 1981; Wiscombe & Warren, 1980a,b). Dozier and Schneider (1981) showed that it was potentially possible to retrieve grain size from AVHRR data. Later, Dozier and Marks (1987) explored the possibility of mapping the spatial distribution of snow grain size with Landsat Thematic Mapper (TM) data, providing also in this case qualitative estimates by mapping snow covered areas into relatively fine-grained new snow and older, coarser-grained snow. Nolin and Dozier (1993) estimated snow grain size using reflectance at 1.04 μm from Airborne Visible/Infrared Imaging Spectrometer (AVIRIS) data. Bourdelles and Fily (1993) used TM and found that the values of grain size retrieved from band 4 at 0.84 μm were lying in the 420–430 μm range, which is much larger than the 145–165 μm grain size obtained from TM5 (1.65 μm) and TM7 (2.22 μm). They noted that retrieved size depends on the radiation–penetration depth, which is wavelength-dependent. Also, Fily et al. (1997) compared the in situ and Landsat TM-retrieved snow grain sizes and found that the in situ optical grain size is very different from the measured one at channels TM5 and TM7, but is close to the measured one at channel TM4. In 2000, Nolin and Dozier proposed a more robust algorithm with respect to the one

proposed in 1993 that integrates across the entire 1.03-μm absorption feature. Li et al. (2001) proposed a technique to retrieve the vertical distribution of the grain size using different penetration of near IR radiation to a snow field depending on the wavelength used for probing snow. Green et al. (2002) used AVIRIS data to map the solid, liquid, and vapor phases of water and quantified the distribution of optical path lengths for ice (related to grain size). Painter and Dozier (2004) discussed relevant snow grain size measurements and comparisons to model results. Also, Painter et al. (2003) mapped fractional snow cover area and fractional snow grain size (optically equivalent grain size) simultaneously. Here, the authors describe and validate a model that retrieves subpixel snow-covered area and effective grain size from Airborne Visible Infrared Imaging Spectrometer (AVIRIS) data over the Mammoth Mountain in California for different snow conditions. Snow spectral endmembers of varying grain size are derived from a radiative transfer model where spectra for vegetation, rock, and soil were collected in the field and laboratory. The estimates of snow-covered area were validated with fine-resolution aerial photographs where the estimates of grain size were validated with stereological analysis of snow samples.

The possibilities of retrieving grain size and concentration of snow impurities from space have been also recently investigated with the launch of the Global Imager (GLI) onboard of the satellite Advanced Earth Observing Satellite II (ADEOS II) on 14 December, 2002 (http://sharaku.eorc.jaxa.jp/ADEOS2/index.html). GLI consisted of an optical sensor observing the reflected solar radiation from the Earth's surface with a multichannel system having wavelengths similar to those used on MODIS. Aoki et al. (2005) reported results regarding the validation of the snow products (grain size and concentration of snow impurities) from the ADEOS II/GLI. Further results are published in the web at http://suzaku.eorc.nasda.go.jp/GLI/cryos/val/GLI_cryos_v2_report.pdf. Unfortunately, the analysis of the retrieval performance can be carried out only for a limited period because on 24 October, 2003 the Japanese Aerospace Exploration Agency (JAXA) stopped receiving data from ADEOS II due to an unknown anomaly. However, preliminary studies were conducted to support the retrieval of the snow properties from GLI. Tanikawa et al. (2002) retrieved snow grain-size and concentration of snow impurities from Airborne Multispectral Scanner (AMSS) images at the visible and near-infrared wavelengths observed over the flat snowfield in eastern Hokkaido, Japan, in February 1998. The estimated snow grain size and the concentration of impurities were found to be consistent with the results of in situ measurements on the snow surface. Again, for snow grain size, measured reflectance in the different near-infrared AMSS channels indicated grain size differences in the vertical profile of the snowpack.

3. Theoretical basis and the retrieval approach

The Semi-Analytical snow Retrieval Algorithm (SARA) developed in this work is based on the Asymptotic Radiative transfer Theory (ART) valid for semi-infinite weakly absorbing media. Correspondent theory is described by Kokhanovsky and Zege (2004) and also at a greater depth by Kokhanovsky (2006). The dense media effects are neglected. However, differently from most of other works related to snow remote sensing, the non-sphericity of grains is taken into account. For this, the fractal model introduced by Macke et al. (1996) is used. This model captures the phase function of crystalline disperse media like snow or ice better than a model using spherical particles (e.g., Kokhanovsky et al., 2005) and it is much more accurate as compared to the model of spherical snow grains used by snow remote sensing community in the past.

The approximate asymptotic theory of snow optical properties developed by Kokhanovsky and Zege (2004) has been validated by using *in situ* measurements of snow reflectance (Kokhanovsky et al., 2005) at the wavelengths of 0.545, 1.050, 1.240, and 2.210 μm, and a high accuracy of the theory was confirmed. The wavelengths specified above coincide with atmospheric windows, where gaseous absorption can be neglected or easily taken into account. In the following, we report a summary of the equations used in this study. For other detailed information regarding the development of the theory in object, we advice the reader to consult www.iup.uni-bremen.de/~alexk/.

The reflection function of a semi-infinite weakly absorbing layer of snow R is modeled in the framework of ART as follows:

$$R(\vartheta_0,\vartheta,\varphi)=R_0(\vartheta_0,\vartheta,\varphi)\exp(-\alpha f(\vartheta_0,\vartheta,\varphi)), \quad (1)$$

where R_0 is the reflection function of a semi-infinite non-absorbing snow layer. The reflection function R is defined as $\pi I(\vartheta_0,\ \vartheta,\ \varphi)/F\ \cos\ \vartheta_0$, where I is the intensity of reflected light, F is the density of the incident light flux, the values of ϑ_0, ϑ, φ are the incidence zenith angle, the observation zenith angle, and the relative azimuth, respectively. This function is proportional to the so-called bi-directional reflection distribution function $\rho(\vartheta_0,\ \vartheta,\ \varphi)$ often used in works on snow remote sensing: $R=\pi\rho$. The function $f(\vartheta_0,\ \vartheta,\ \varphi)$ is given as follows:

$$f(\vartheta_0,\vartheta,\varphi)=\frac{K_0(\vartheta_0)K_0(\vartheta)}{R_0(\vartheta_0,\vartheta,\varphi)}, \quad (2)$$

where $K_0\ (\vartheta_0)$ is called the escape function in radiative transfer theory and can be approximated by the following expression (Kokhanovsky et al., 2003):

$$K_0(\xi)=\frac{3}{7}(1+2\xi), \quad (3)$$

where $\xi=\cos\vartheta_0$. Eq. (3) is valid with accuracy better than 2% at $\cos\vartheta_0$ larger than or equal to 0.2 (Kokhanovsky, 2006). The escape function describes the normalized angular distribution of photons escaping a semi-infinite nonabsorbing medium with sources located in the medium at infinity. Further details are given by Van de Hulst (1980).

The value of α in Eq. (1) is given by $\alpha=A\sqrt{\gamma d}$ (Kokhanovsky & Zege, 2004) where $A\cong 3.6$, $\gamma=4\pi\chi/\lambda$, χ is the imaginary part of the refractive index of ice, λ is the wavelength, and d is the effective grain size (EGS) defined as $d=6<V>/<\Sigma>$, being $<V>$ and $<\Sigma>$, respectively, the average volume and surface area of particles. For monodisperse spheres,

EGS coincides with a diameter. Combining the equations, the snow spectral reflection function can be written as follows:

$$R(\vartheta_0,\vartheta,\varphi)=R_0(\vartheta_0,\vartheta,\varphi)\exp(-B\sqrt{\gamma d}), \tag{4}$$

where

$$B=\frac{\varepsilon(1+\cos\vartheta_0)(1+\cos\vartheta)}{R_0(\vartheta_0,\vartheta,\varphi)} \tag{5}$$

and $\varepsilon=9A/49$ or $\varepsilon\approx 0.66$ for fractal grains. In such a way the snow reflection function is parameterized in terms of EGS d, the reflection function of a semi-infinite snow layer at zero absorption R_0, and the angular factor B, which accounts for the influence of geometry (and also the shape of grains) on the level of light absorption by snow. General Eqs. (4) and (5) are valid for arbitrary shapes of snow grains. The constant B and the value of R_0 are shape dependent (Kokhanovsky & Zege, 2004).

Eq. (4) can be used to derive EGS as follows:

$$d=\frac{1}{B^2\gamma}\ln^2\left(\frac{R}{R_0}\right). \tag{6}$$

The value of R_0 can be computed, e.g., from the correspondent radiative transfer code, Look-Up-Tables (see, e.g., Kokhanovsky & Nauss, 2006 and also www.iup.physik.uni-bremen.de/~alexk) or from various approximations. In this work the following approximate analytical result is used (Kokhanovsky, 2005):

$$R_0(\vartheta_0,\vartheta,\varphi)=\frac{a+b(\xi+\eta)+c\xi\eta+p(\theta)}{4(\xi+\eta)}, \tag{7}$$

where $a=1.247$, $b=1.186$ and $c=5.157$. The function $p(\theta)$ is the snow grain phase function and it can be approximated in the model of fractal crystals as follows(Kokhanovsky, 2005):

$$p(\theta)=11.1e^{-0.087\theta}+1.1e^{-0.014\theta}, \tag{8}$$

where

$$\theta=\cos^{-1}(-\xi\eta+\sqrt{(1-\xi^2)(1-\eta^2)}\cos\varphi), \tag{9}$$

is the scattering angle in degrees and ξ and η being, respectively, $\cos\vartheta_0$ and $\cos\vartheta$.

The accuracy of Eqs. (7) and (8) has been studied by Kokhanovsky (2005) and depends on the observation angle. In particular, it is smaller than 3% at nadir observation and solar zenith angles smaller than 78°. The error increases with zenith observation angle. However, it remains smaller than 10% at arbitrary azimuth and $\vartheta_0<35°$, $\vartheta<78°$ The errors of this approximation are smaller as compared to those occurring using a spherical snow grain shape model.

Simple analytical Eqs. (5)–(9) constitute the basis of SARA, which enables the determination of d from measurements of the snow reflection function R in the near-infrared. Knowing EGS, one can retrieve the concentration of pollutants (for a given model of a pollutant spectral refractive index, chemical composition, and microstructure) as described by Kokhanovsky and Zege (2004). Therefore, EGS is determined using a system of analytical equations shown above, which can be collected in just one simple formula:

$$d=\frac{\left(a+b(\xi+\eta)^2+c\xi\eta+p(\theta)\right)^2}{16\gamma\varepsilon^2(1+\xi)^2(1+\eta)^2(\xi+\eta)^2}\ln^2\times\left[\frac{4(\xi+\eta)R(\xi,\eta,\varphi)}{a+b(\xi+\eta)+c\xi\eta+p(\theta)}\right], \tag{10}$$

where R is the measured reflection function in the near IR. The simple check of the model developed is the determination of EGS for different combinations of (ξ,η,φ). The derived values of EGS must not differ considerably.

Similar simple expressions for EGS can be derived, if the plane (r_p) or spherical (r_s) albedos (see Kokhanovsky & Zege, 2004 for definitions of the pair (r_p, r_s)) are measured (instead of R). Following Kokhanovsky and Zege (2004), we write

$$r_p=e^{-AK_0(\xi)\sqrt{\gamma d}}, \tag{11}$$

$$r_s=e^{-A\sqrt{\gamma d}}. \tag{12}$$

Therefore, it follows for EGS:

$$d=\frac{1}{\gamma A^2K_0^2(\xi)}\ln^2(r_p), \tag{13}$$

$$d=\frac{1}{\gamma A^2}\ln^2(r_s). \tag{14}$$

The accuracy of Eq. (12) is studied elsewhere (Kokhanovsky & Zege, 2004) where the authors point out that experimental data can be explained by ART for a wide spectral range starting from UV until approximately 1.4 μm. Generally, Eq. (12) is valid for the spherical albedo larger than 30%. For smaller albedo, the accuracy decreases. For very large grains Eq. (12) may become not applicable already at 1.4 μm. On the other hand, it might be applied at 2.2 μm, if grains are small.

The values of EGS determined from the spherical or plane albedo measurements can be derived in the assumption of equivalent spherical grains. This is not the case for measurements of the reflection function because then the derived value of EGS starts to depend on angles (ϑ_0, ϑ, φ) because incorrect assumptions on the shape of particles, which is against the physics of the problem (Grenfell et al., 2005; Neshyba et al., 2003). The simple technique to check the applicability of the spherical model is to prove that EGS retrieved from albedo and reflection function measurements coincide. The degree of deviation can be considered as a proxy for the validity of the model. The same applies to the retrieval technique proposed here.

As an example of the spherical albedo derived from Eq. (12), Fig. 1a shows the behavior of the spherical albedo as a function of the wavelength between 0.4 and 2.4 μm for different values of EGS (100, 200, 400 and 800 μm) under the hypothesis of fractal particles. It follows from this figure that the grain size might be indeed easily obtained from measurements at 1.2 μm. This channel is almost free of gaseous absorption. The dashed

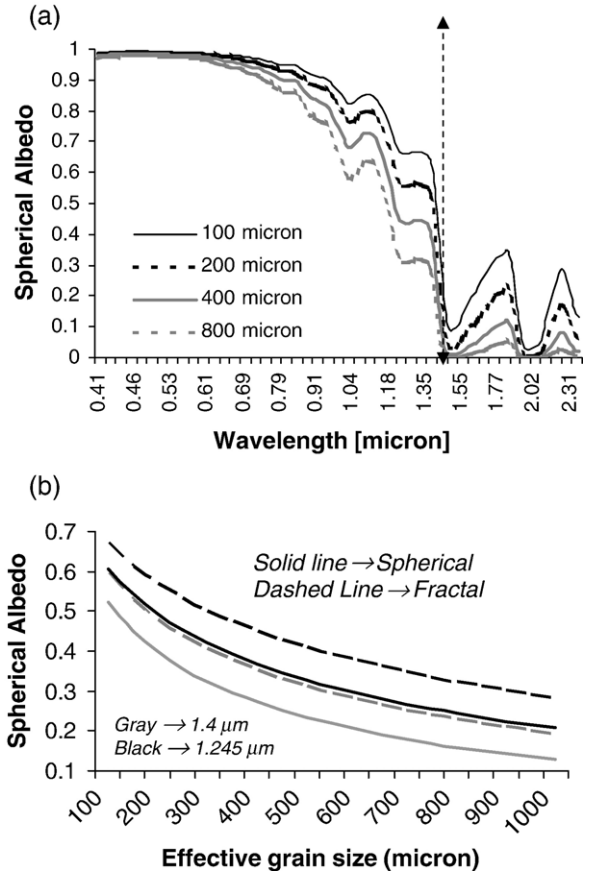

Fig. 1. a) Spherical albedo vs. wavelength computed with Eq. (12) for different grain size dimensions (fractal particles) and b) Spherical albedo vs. grain size at 1.245 and 1.4 μm for spherical and fractal particles assumptions. Note that in the case of spherical particles the grain size is the particle diameter.

line with the two arrows area denotes the fact that the equation used to compute the spherical albedo is valid up to 1.4 μm. Fig. 1b plots the albedo versus grain size obtained with Eq. (12) at the wavelengths of 1.245 and 1.4 μm in cases of spherical and fractal particles assumptions. The values of A used in the case of fractal particles is 3.63 and the value used in the case of spherical particles is 4.53 (Kokhanovsky & Zege, 2004). Note that in the case of spherical particles the effective grain size represents the particle diameter. From the figure we observe that the difference between the spherical albedos obtained in the case of fractal and spherical particles is significant in the near IR. This points out that the hypothesis of spherical particles can affect substantially the values of the retrieved effective grain size. In particular, it follows from Fig. 1 that EGS is underestimated if the model of spherical snow grains is used. The spherical albedo of snow in the visible is close to one independently on the size and shape of grains (omitted in the figure).

4. Local scale validation and sensitivity to the wavelength choice

Before applying the retrieval procedure to space-borne measured data, we retrieve EGS at local scale by using ground based observations. Measurements of spectral plane albedo in the wavelength region of 0.35–2.500 μm were carried out together with snow pit work on a flat snowfield in eastern Hokkaido, Japan on February 23rd, 1998 (Aoki et al., 2000). Here the authors found that the optically equivalent snow grain size is of the order of a branch width of dendrites or of a dimension of narrower portion of broken crystals, using the model of spherical scatterers. This size was smaller than both the mean grain size and the effective grain size obtained from micrographs by image processing.

To validate SARA, we retrieve the value of EGS using Eq. (14) applied to measurements of the plane albedo at the solar zenith angle 57 degrees collected at the wavelengths of 1.1, 1.245 and 1.4 μm. Retrieved values are compared with those obtained from snow pit work, image processing and spectral albedo fitting published in the original work by Aoki et al. (2000). The symbols used here with a description of the different types of grain size considered for the comparison are reported in Table 1 for reader's convenience. In the table, d_1 and d_2 represent the values of grain size of snow surface obtained from snow pit data with d_1 being the length of the major axis of crystals or dendrites, and d_2 the branch width of dendrites or the dimension of the narrower portion of broken crystals; the mean

Table 1
Symbols and description of the different types of grain size considered for the comparison

Symbol	Definition	Source
d_1	Length of the major axis of crystals or dendrites	Snow pit observation
d_2	Branch width of dendrites or the dimension of the narrower portion of broken crystals	Snow pit observation
d_{image}	Mean diameter	Image processing
$d_{effimage}$	Effective diameter	Image processing
d_{VA}	Diameter of the equal volume/surface area sphere	Value of the diameter of the equal volume/area sphere obtained using the approach suggested by Grenfell and Warren (1999)
d_{fit}	Fitting diameter in the original work by Aoki et al. (2000), indicate that plane albedo data have been used	Fitting technique
$d_{fit\_sph\_wv}$	Fitting diameter in this study by assuming spherical particles at wavelength wv	Fitting technique
$d_{fit\_fract\_wv}$	Fitting grain size in this study by assuming fractal particles at wavelength wv	Fitting technique

Table 2
Values of grain size (μm) of snow surface obtained from snow pit work (d_1 and d_2), image processing (d_{image}, $d_{effimage}$ and d_{VA}) and spectral albedo fitting in (Aoki et al., 2000)

Date	d_1	d_2	d_{image}	$d_{effimage}$	d_{VA}	d_{fit}
Feb. 22	200–1500	100–200	178	280	84	70
Feb. 23	600–1000	100–300	218	326	114	110
Feb. 24	200–1000	100–300	264	390	154	130
Feb. 25	500–1500	100–300	286	440	192	170

Table 3
Values of grain size derived from the Eq. (14) by fitting the plane albedo measured in Aoki et al. (2000) considering spherical particles (d_{fit_sph}) or fractal particles (d_{fit_fract})

Date	$d_{fit\_sph\_1.1}$ [μm]	$d_{fit\_fract\_1.1}$ [μm]	$d_{fit\_sph\_1.25}$ [μm]	$d_{fit\_fract\_1.25}$ [μm]	$d_{fit\_sph\_1.4}$ [μm]	$d_{fit\_fract\_1.4}$ [μm]	$d_{fit\_sph\_Av}$ [μm]	$d_{fit\_fract\_Av}$ [μm]
Feb. 22	95	147	103	161	88	137	100	148
Feb. 23	182	285	155	241	143	226	176	273
Feb. 24	270	421	213	333	190	296	208	326
Feb. 25	336	523	293	457	210	326	258	403

The numbers 1.1, 1.25 and 1.4 at the subscript indicates the wavelength used for deriving the grain size. Note that values of diameters are reported for a better comparison with the fractal grain size EGS. The two final columns report the grain size obtained by averaging the results from the previous columns.

diameter d_{image} represents the values obtained from the circle equivalent diameter calculated from the projected area by means of a sphere-separating algorithm; the effective diameter $d_{effimage}$ is determined in the way similar to d_{image} except the area-weighting averaging is used (Hansen & Travis, 1974). The value of d_{VA} represents the value of the diameter of the equal volume/area sphere (Grenfell & Warren, 1999; Neshyba et al., 2003) and, finally, d_{fit} represents the values obtained from the spherical albedo fitting performed by Aoki et al. (2000). It is expected (Kokhanovsky & Zege, 2004) on general grounds that d_{fit} must be close to d_{VA}. However, the measurement of d_{VA} in snow *in situ*, e.g., using the methane adsorption technique, is a complex and time-demanding procedure (Dominé et al., 2006; Legagneux et al., 2002), which is rarely performed.

Results obtained under the assumptions of both fractal and spherical particles are reported below. The choice of the wavelengths for our retrieval is mainly dictated by the fact that the equation that we use for retrieving grain size (Eq. (14)) is valid for wavelengths smaller than 1.4 μm and the results reported in Aoki et al. (2000) are obtained by fitting the albedo measured above 1.4 μm. A study extending the capabilities of SARA above 1.4 μm is under progress.

Results published in Aoki et al. (2000) are reported in Table 2 for reader's convenience. Table 3 shows the results obtained in this study with $d_{fit\_sph\_wv}$ and $d_{fit\_fract\_wv}$ representing, respectively, the values of the diameter and the dimension of the grain size retrieved in this study by using spherical ($d_{fit\_sph\_wv}$) or fractal particles ($d_{fit\_fract\_wv}$) assumptions.

Results reported in Tables 2 and 3 are plotted as graphs in Fig. 2. Here, the values of grain size retrieved with the method proposed in this study under the assumption of (a) spherical and (b) fractal particles and those reported in Aoki et al. (2000) are displayed. Lines represent the values retrieved in this study with $d_{1.1}$, $d_{1.245}$ and $d_{1.4}$ referring to the values obtained by using the values of the albedo collected, respectively, at 1.1, 1.245 and 1.4 μm. The value of d_{Av} is obtained by averaging the values retrieved at the different wavelengths. The values of measured grain size and those retrieved in Aoki et al. (2000) are plotted as dots with diamonds representing d_{image}, triangles $d_{effimage}$, circles $d_{V/A}$ and squares the values d_{fit} fitted in the original paper. Tables 4 and 5 show the relative percentage difference between the values of effective grain size retrieved in this study and the values d_{fit} (Table 4) and $d_{V/A}$ (Table 5) reported in Aoki et al. (2000).

We observe that the values of grain size derived in this study (Fig. 2a) are generally closer to those obtained by Aoki et al. (2000), if the spherical model is used. However, they are higher than those fitted by Aoki et al. (2000). On the other hand, the values $d_{fit\_sph\_1.4}$ fitted in this study are close to the values d_{VA} in Aoki et al. (2000). In order to explain this discrepancy we must consider 1) the penetration into the snowpack at different wavelengths and 2) the vertical distribution of measured grain size. It is known that longer wavelengths carry information for a shallower layer of the snow (e.g. Li et al., 2001), and this can be

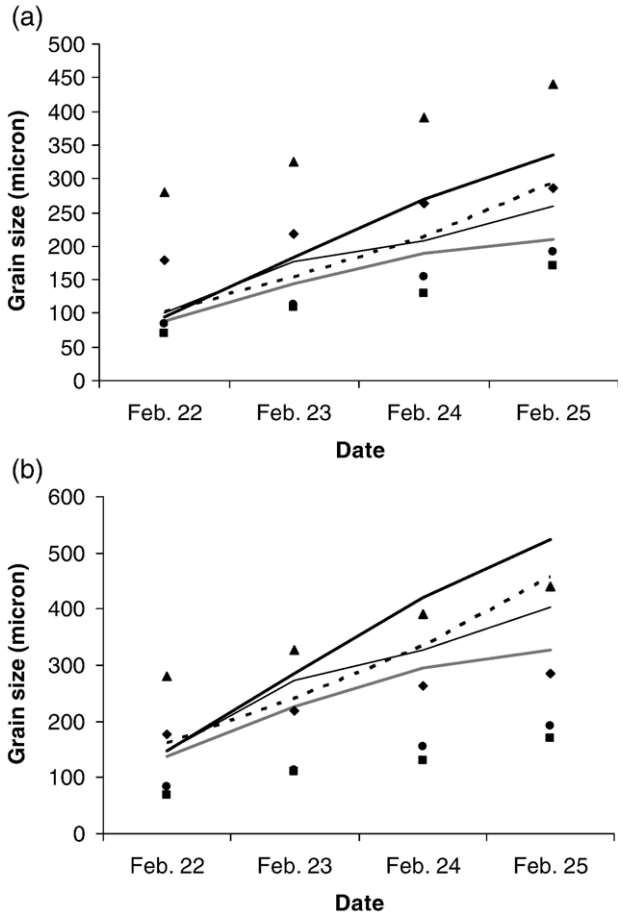

Fig. 2. Comparison between values of grain size retrieved with the method proposed in this study under the assumption of (a) spherical and (b) fractal particles and those reported in Aoki et al. (2000) (Table 3). Lines represent the values retrieved in this study at 1.1 (cont. black thick line), 1.245 (dashed black line) and 1.4 μm (cont. gray thick line). The value of d_{Av} is obtained by averaging the values retrieved at the different wavelengths (solid thin black line). The values retrieved in Aoki et al. (2000) are plotted with diamonds representing d_{image}, triangles ($d_{effimage}$), circles (d_{VA}) and squares the values fitted in the original paper d_{fit}.

Table 4
Relative percentage difference between the values of effective grain size retrieved in this study and the values d_{fit} fitted in Aoki et al. (2000)

Date	$\Delta d_{fit\_sph\_1.1}$	$\Delta d_{fit\_fract\_1.1}$	$\Delta d_{fit\_sph\_1.2}$	$\Delta d_{fit\_fract\_1.25}$	$\Delta d_{fit\_sph\_1.4}$	$\Delta d_{fit\_fract\_1.4}$	$\Delta d_{fit\_sph\_Av}$	$\Delta d_{fit\_fract\_Av}$
	%	%	%	%	%	%	%	%
Feb. 22	35.71	110.71	48.21	130.36	26.79	96.43	42.86	112.50
Feb. 23	65.91	159.09	40.91	119.32	30.68	105.68	60.23	148.86
Feb. 24	107.69	224.04	64.42	156.73	46.15	127.88	60.58	150.96
Feb. 25	97.79	208.09	72.79	169.12	23.53	91.91	52.21	137.50

mainly explained considering the behavior of imaginary part of refractive index of ice with the wavelength. The light absorption by ice is weaker at shorter wavelength and, as a consequence, the sunlight penetrates into deeper layers, with the reflected light containing information on snow from a relatively deeper layer. On the other hand, at longer wavelengths the light absorption is stronger and the reflected light contains information from the top layer. Now we take into account the fact that the measured snow grain sizes at the surface are smaller than those at the deeper layers (Aoki et al., 2000; Tanikawa et al., 2002) and that grain size values in Aoki et al. (2000) are retrieved by fitting the values of albedo measured above 1.4 μm. The values derived in this study are obtained by using the values of albedo collected at 1.1, 1.25 or 1.4 μm wavelength. As a consequence, the values retrieved by Aoki et al. (2000) correspond to the upper part of the snowpack and consist of smaller grain size where the values retrieved in this study involves deeper layers and, because of this, are bigger. This is also confirmed by the fact that the values of grain size retrieved in this study decrease (except on February 22nd) as the wavelength increases (see Figs. 1 and 2). Results retrieved by us at 1.4 μm are just 6–26% larger (depending on the day) as compared to those reported by Aoki et al. (2000) using the full radiative transfer model. From Fig. 2 we also observe that the values of optically equivalent grain size retrieved for fractal particles better agree with the values of the diameter d_{image} obtained by image processing techniques. Studies to investigate the reason of the observed trend are under progress.

5. Retrieval of grain size from MODIS data

In this section we show the results obtained by applying the inversion procedure to MODIS data. However, before proceeding with the application and validation of the retrieval technique, we introduce and briefly describe the products derived from MODIS which will be used. They consist of 3 different products providing values of reflectance at different wavelengths, maps of snow cover area and cloud areas and the information regarding the solar illumination and instrument viewing geometry angles.

5.1. MODIS products used for the retrieval

MODIS is an instrument flying aboard the TERRA and AQUA satellites collecting data in 36 spectral bands (http://modis.gsfc.nasa.gov/about/) ranging in wavelength from 0.4 μm to 14.4 μm. The first MODIS instrument is integrated on TERRA and it was successfully launched on December 18, 1999. The second MODIS instrument is integrated on AQUA and it was successfully launched on May 4, 2002.

5.1.1. MODIS surface reflectance

The MODIS Surface Reflectance product (denoted as MOD09GHK for TERRA and MYD09GHK for AQUA gives an estimate of the surface spectral reflectance as it would have been measured at ground level. A correction scheme compensating for the effects of atmospheric gases, aerosols, and thin cirrus clouds is applied. It uses input from several other MODIS products: Bidirectional Reflectance Distribution Function (BRDF)/Albedo Product (MOD43), Atmospheric Profiles (MOD07) for ozone, Total Precipitable Water (MOD05) for water vapor, Aerosol Product (MOD04) for aerosols, and MODIS band 26 for cirrus clouds. The best available ancillary or climatology data are used if these MODIS-specific inputs are unavailable. Further information about the product can be found at http://edcdaac.usgs.gov/modis/mod09ghkv4.asp.

5.1.2. MODIS snow cover area

Daily snow cover product derived from the MODIS sensor (MOD10A1 for TERRA and MYD10A1 for AQUA) gridded to a spatial resolution of 500 m is used here. The daily data selected from multiple observations in a MOD10A1 (or MYD10A1) cell is the observation acquired nearest nadir and having the greatest coverage of the grid cell. The snow cover area products are tiles

Table 5
Relative percentage difference between the values of effective grain size retrieved in this study and the values $d_{V/A}$ reported in Aoki et al. (2000)

Date	$\Delta d_{fit\_sph\_1.1}$	$\Delta d_{fit\_fract\_1.1}$	$\Delta d_{fit\_sph\_1.2}$	$\Delta d_{fit\_fract\_1.25}$	$\Delta d_{fit\_sph\_1.4}$	$\Delta d_{fit\_fract\_1.4}$	$\Delta d_{fit\_sph\_Av}$	$\Delta d_{fit\_fract\_Av}$
	%	%	%	%	%	%	%	%
Feb. 22	13.09	75.59	23.51	91.96	5.65	63.69	19.04	77.08
Feb. 23	60.09	150.05	35.96	111.62	26.09	98.46	54.60	140.13
Feb. 24	75.32	173.53	38.79	116.72	23.37	92.37	35.55	111.85
Feb. 25	75.13	172.78	52.99	138.28	9.37	69.92	34.76	110.28

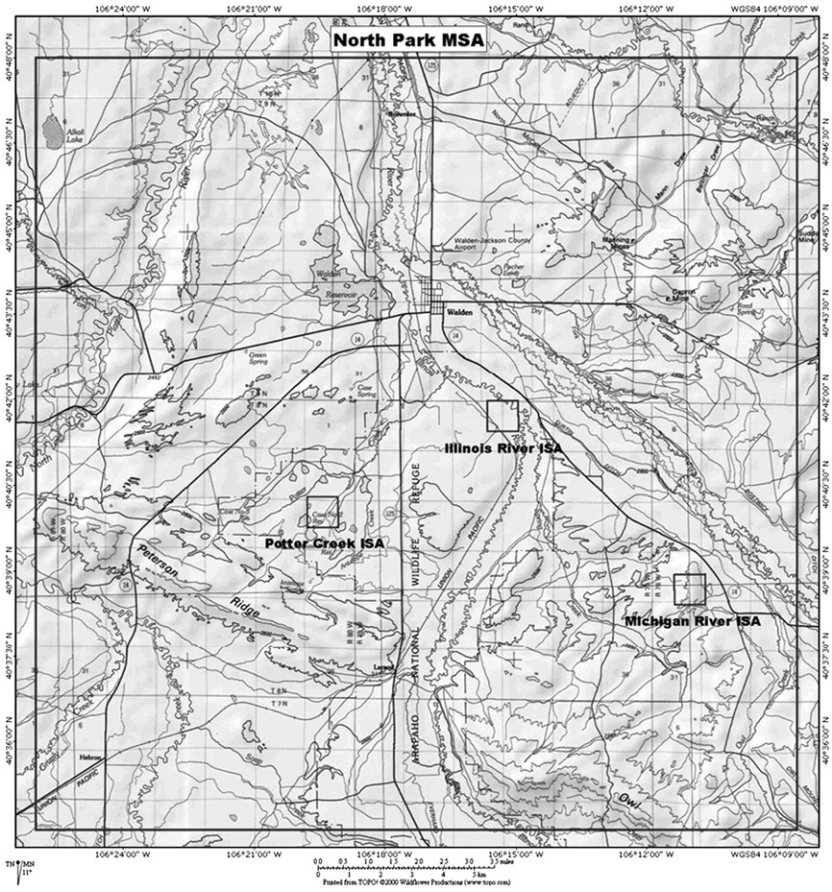

Fig. 3. The 25-km × 25-km North Park Study Area. Nested within the area are three 1-km × 1-km Intensive Study Areas: Potter Creek ISA, Illinois River ISA, and Michigan River ISA (Courtesy: http://www.nohrsc.nws.gov/(cline/clp/field_exp/clpx_plan/figures/CLPX_plan_fig5.htm).

of data gridded in the sinusoidal projection. Tiles are approximately 1200 × 1200 km in area. The same product contains also a cloud mask which is used to exclude those pixels containing clouds from the computation of grain size. In some cases cloud covered areas might be misclassified as snow and vice-versa with the error between snow/cloud detection is estimated to be at maximum 3% in a swath for the 500 m resolution product (Riggs, 2006). Further information can be found at http://modis-snow-ice.gsfc.nasa.gov/.

5.1.3. MODIS Global Geolocation Angle

The MODIS Global Geo-location Angle (MODMGGAD, MYDMGGAD) product is used for extracting information about solar illumination and instrument viewing geometry angles (solar and sensor azimuth and zenith angles). Geometric information for each sensor observation is stored on a geolocated grid with Level 2 geophysical parameters stored as Level 2G (gridded) products. The multiple observations stored in the L2G grids are examined by the Level 3 processes to extract only the most relevant observations per grid cell. Please, see http://edcdaac.usgs.gov/modis/dataproducts.asp#modmgga for further details.

5.2. Retrieval of grain size from satellite data

The values of grain size retrieved with space-borne data are compared with those measured on the field during the Cold Land Processes Experiment (CLPX-1), Colorado in 2003 by using a microscope with 8 × 30 optics (http://www.nohrsc.nws.gov/~cline/clpx.html and http://nsidc.org/data/clpx). One of the tasks of CLPX-1 was to understand at what scale the spatial variability of snow characteristics control fluxes, the transformation of water and energy and if remote sensing can resolve the variability at these scales. Within this framework, intensive ground, airborne and space-borne data were collected in several study areas in Colorado, central Rocky Mountain of the western United States, during February and March of 2002 and 2003. CLPX-1 measurements provide a useful data set to validate the retrieval technique here proposed. Data collected at North Park MSA during the third Intensive Observation Period (IOP3) on February 19–25, 2003 include detailed measurements of snow parameters along the vertical profile, including grain size. Similar to the dirty snow effects, thin snow can influence the value of the reflectance (e.g. Nolin & Dozier, 2000). As a consequence, we did not consider all grain size measurements collected from snow pits where snow depth was less than 20 cm. The upper left corner coordinates of the area considered for the retrieval (and including North Park MSA) are 41° N latitude and −106.5° W longitude where the coordinates of the lower right corner are 40.5° N latitude and −106° W longitude. The coordinates of the corners of the North Park MSA are the following: 40°48′00″ N and −106°26′00″ W for the upper left corner, 40°34′30″ N and −106°26′0″ W for the lower left

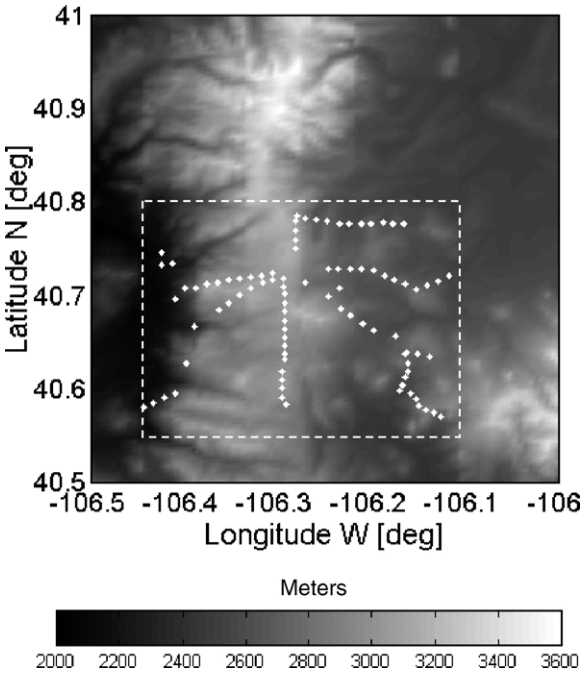

Fig. 4. DEM of the area selected for the validation of grain size retrieval, including the North Park MSA (bounded by the square box). The locations of the grain size ground measurements are also reported as dots.

corner, 40°48′00″ N and −106°08′3″ W for the upper right corner and 40°34′30″ N and −106°08′30″ W for the lower right corner. As a reference, Fig. 3 shows the 25-km×25-km North Park Study Area. Nested within the area are visible three 1-km×1-km Intensive Study Areas: Potter Creek ISA, Illinois River ISA, and Michigan River ISA (Courtesy: http://www.nohrsc.nws.gov/~cline/clp/field_exp/clpx_plan/figures/CLPX_plan_fig5.htm). Fig. 4 shows the Digital Elevation Model (DEM) at 500 m resolution of the test area. The 500 m resolution DEM was obtained from the Pennsylvania State University (PSU) Center for Environmental Informatics Database (http://dbwww.essc.psu.edu) and it was derived from the 3″ DEM distributed by the USGS. Fig. 4 also shows the locations of the measurements of snow grain size performed on the ground. The area where grain size measurements were performed is located at high elevation and it is relatively flat, with a mean elevation of 2499 m, a range of 312 m and a standard deviation of 45 m. In this study we will not consider the correction of the satellite measured reflectance for local incidence angle but this analysis is one of the main tasks of the future work.

We also analyzed the distribution of forest cover within the area of interest, to account for the spectral mixing due to the presence of the forest (e.g. Painter et al., 2003). Fig. 5 shows the forest map classification for the area of interest obtained from the Global Land Cover Facility of the University of Maryland (http://glcf.umiacs.umd.edu/index.shtml). White color corresponds to a forest cover fraction between 0% and 5%, light gray to a fraction between 5% and 10%, medium gray to a fraction between 10% and 40%, dark gray to a fraction between 40% and 60% and black to a fraction greater than 60%. We see that only the right side of the total area shows significant presence of forest coverage where the area including the CLPX-1 North Park MSA has a very low forest cover fraction (less than 5%).

In Fig. 6 we show the maps of the retrieved values of grain size on February 19, 2003 from both MODIS-TERRA (crossing the equator at 10:30 a.m. local time) and MODIS-AQUA (crossing the equator at 1:30 p.m. local time) instruments. White values represent areas covered by clouds. The day was selected because it was the one showing the most extended free-cloud area. The effect of the forest is well observable (high values of retrieved grain size matching the high values of forest density) and it is consistent with measurements performed by both satellites. Here what happens is that the presence of the forest within the observed area reduces the value of the measured reflectance and, without any further correction, the algorithm tends to overestimate the values of grain size to match the observed and computed values of reflectance. Techniques for correcting for the presence of sub-pixel forest and bare ground have been proposed in the literature (e.g. Kaufman et al., 2002; Painter et al., 2003). However, as it is possible to observe from Fig. 5, the area including the validation site is mostly free of forest and, therefore, this aspect will not be considered here. Fig. 7 shows the same as Fig. 6 but for February 19, 2003.

The comparison of the maps derived from the morning and afternoon passes shows that the values of grain size derived from the morning pass are, generally, lower than those derived from the afternoon pass. Besides, the spatial distribution of grain size values derived from the morning shows less variability than that derived from the afternoon pass. The mean values of the retrieved grain size within the North Park MSA are, respectively, $d_{\text{mean\_TERRA}}=185$ μm (around 10:30 a.m.), $d_{\text{mean\_AQUA}}=430$ μm (around 1:30 p.m.) with standard deviations $\sigma_{\text{mean\_AQUA}}=187$ μm and $\sigma_{\text{mean\_TERRA}}=43$ μm (fractal assumption). The larger retrieved values of grain size for AQUA are in agreement with experimental observations

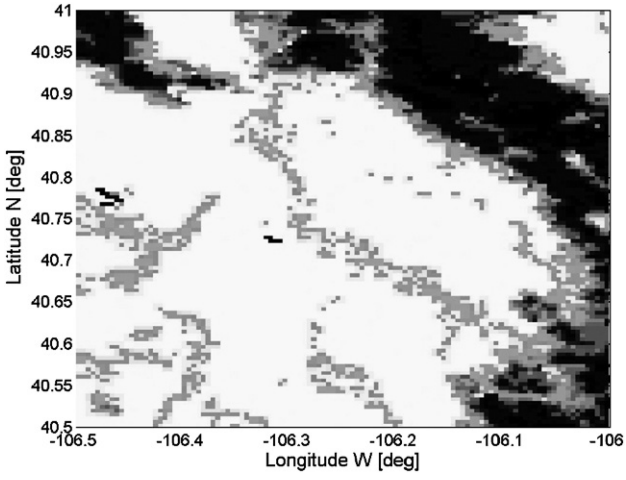

Fig. 5. Forest map classification of the test area derived from the Global Land Cover Facility of the University of Maryland (http://glcf.umiacs.umd.edu/index.shtml). White color corresponds to a forest cover fraction between 0% and 5%, light gray to a fraction between 5% and 10%, medium gray to a fraction between 10% and 40%, dark gray to a fraction between 40% and 60% and black to a fraction greater than 60%.

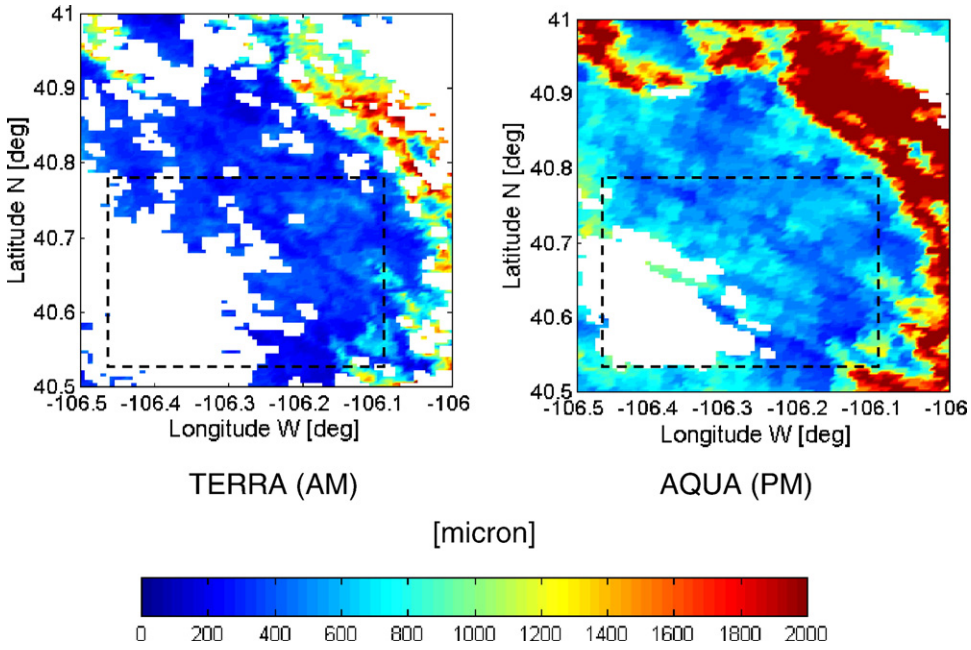

Fig. 6. Effective grain size retrieved from MODIS TERRA (AM pass) and MODIS AQUA (PM pass) on February 19, 2003 over the validation area including the North Park MSA, denoted by the square box. White color corresponds to cloudy area.

reporting that on the morning of February 19, 2003 a snowfall occurred over several areas within the CLPX-1 area. The occurrence of snowfall justifies the smaller average value of the grain size retrieved from the morning pass data (TERRA) together with the relatively homogeneous spatial distribution. As the metamorphism of grain size evolves the grain sizes become bigger and bigger during the afternoon. Nevertheless, metamorphism may not be the only cause of the observed differences. We have indeed to consider that considerable jump in effective grain size does not tend to occur over a short period in case of dry snow. Besides, air temperatures in North Park in February are generally not warm enough to support the observed increase. If we observe the systematic increase in retrieved grain size over the forested regions (see Fig. 7) we can assume that the observed differences between morning and afternoon retrieved grain size might be likely due to differences in atmospheric correction, calibration, and perhaps viewing geometry as well as pixel size. As an example, Fig. 8 shows the differences (in degrees) between TERRA (morning) and AQUA (afternoon) (a) Solar Zenith, (b) Solar Azimuth

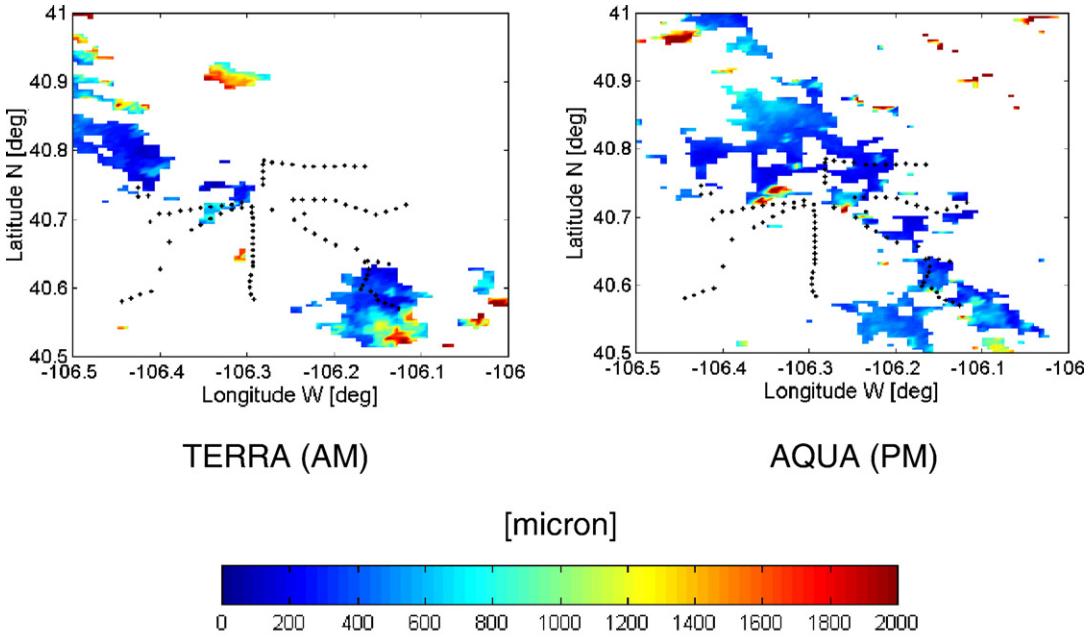

Fig. 7. Grain size values retrieved from MODIS-TERRA vs. those retrieved from MODIS-AQUA on February 19, 2003.

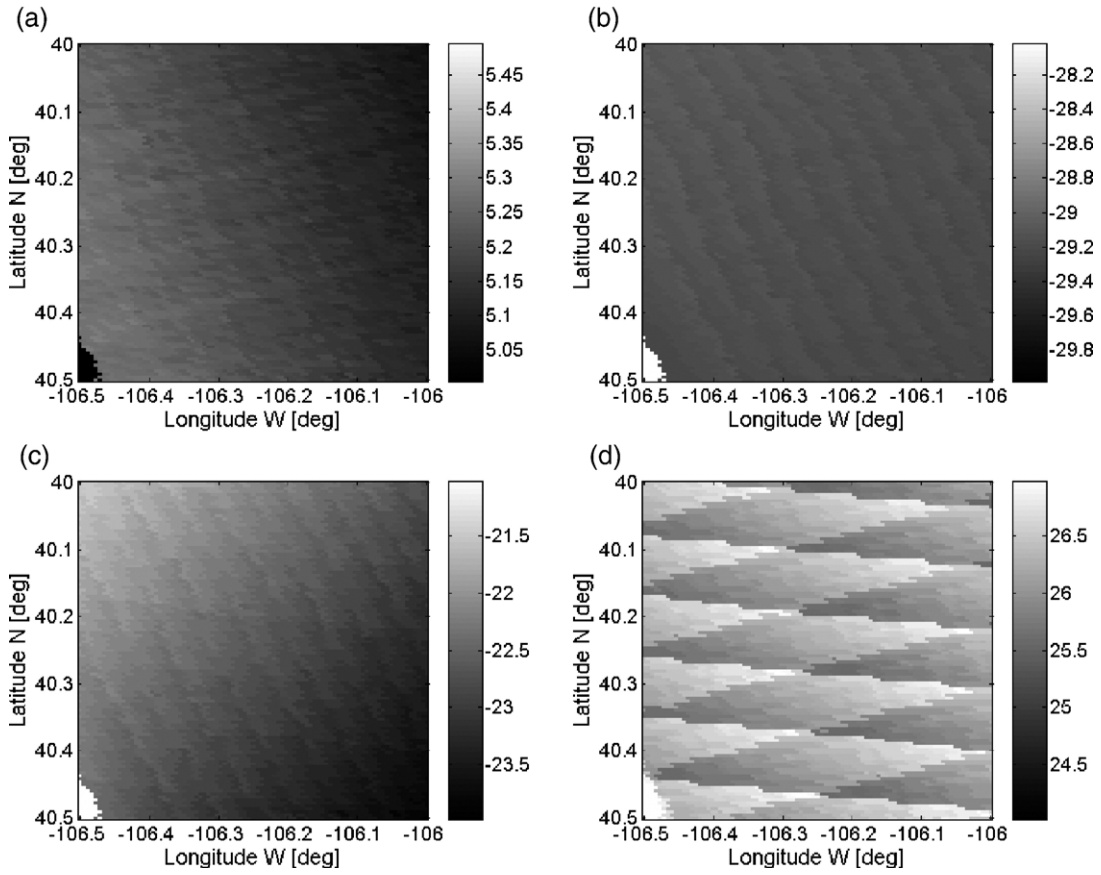

Fig. 8. Differences between TERRA and AQUA (a) Solar Zenith, (b) Solar Azimuth (c) Sensor Zenith and (d) Sensor Azimuth values over the CLPX-1 study area on February 22, 2003.

(c) Sensor Zenith and (d) Sensor Azimuth values over the CLPX-1 study area on February 22, 2003. Fig. 9 shows the values of grain size retrieved from the values of the surface reflectance derived from MODIS data flying on the TERRA satellite vs. those retrieved from values of reflectance derived from MODIS data flying on the AQUA satellite on February 19, 2003. The regression coefficient ($R = d_{\mathrm{TERRA}} / d_{\mathrm{MODIS}}$) is 0.53. From the map of the DEM and of the forest cover density we noticed that, generally, high values of grain size correspond to low elevation and/or high density forested areas. Unfortunately, no measurement is available on those areas and, hence, we can only consider that this is physically reasonable because at low altitudes grains tend to bound each other as a consequence of the strong diurnal temperature gradients. In the case of the forested areas the high values of retrieved grain size might be due to the effect of the forest on the measured reflectance and to the evolution of grain size in forested areas (Fig. 9). Differences obtained from the two MODIS instruments might be also due to different calibration and uncertainty related to atmospheric effects.

Measurements of grain size along the short and long axes were carried out for each class of Small, Medium and Large crystals along the vertical profile of the snowpack at the locations displayed in Fig. 4 on February 22, 2003 (data available at http://nsidc.org/data/nsidc-0176.html). Because of the presence of clouds on February 22, 2003 we can only compare the measured values of grain size with those retrieved from MODIS data acquired on February 21 and, eventually, February 20, 2003. When possible, observations from February 21, 2003 were used because closer in time to the date of the ground measurements. Also, the area of interest was covered by clouds on February 23, 2003, making it impossible to compare values of retrieved grain size successive to the date of ground

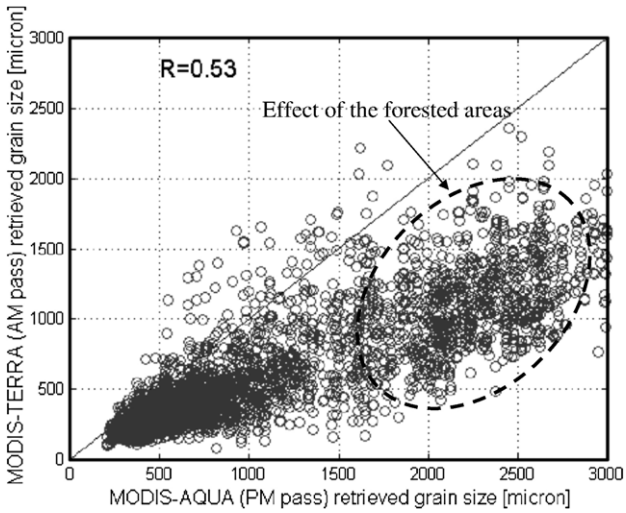

Fig. 9. MODIS-AQUA vs. MODIS-TERRA retrieved grain size.

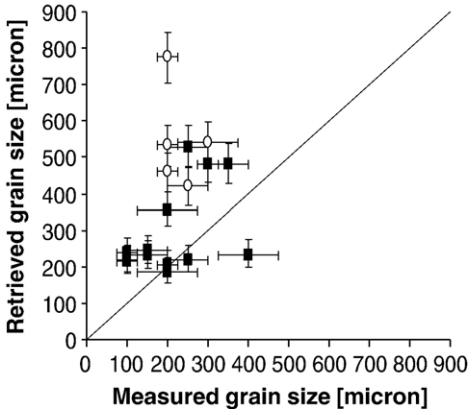

Fig. 10. Comparison between retrieved and measured grain size values. The error bars along the x-axis represent the values along the short and long axes. The error bars along the y-axis represent the variation of the grain size due to a variation of the reflectance of ±5%. Black squares refer to grain size measurements carried out on February 22, 2003 where white circles to grain size values collected on February 21, 2003.

measurements. Fig. 10 shows the comparison between the values of grain size retrieved from MODIS data and those obtained by averaging the measurements along the short and long axes of the crystals belonging to the small class collected from the top layer of the snowpack. Usually, the thickness of the layer in which grain size measurements were performed was of the order of 5–10 cm, much greater than the geometric depth estimated in the Table 2 of Nolin and Dozier (2000). In the figure, the error bars refer to a measurement error on the grain size of 100 μm. Also, white circles refer to data acquired by MODIS flying on the AQUA satellite where black squares refer to those acquired by the MODIS flying on the TERRA satellite. The average differences (Δ, average of the absolute difference between retrieved and measured values) and regression coefficients (e.g., $d_{meas}=Rd_{retr}$) are, respectively, $\Delta=178.4$ μm and $R=0.28$ in the case of the data measured by the MODIS-AQUA and $\Delta=229.9$ μm and $R=0.38$ in the case of the MODIS-TERRA.

6. Discussion on the accuracy and retrieval uncertainty

The accuracy of the snow grain size product is driven by many factors (e.g., poor spatial coverage by ground measurements, time difference, atmospheric effects, snow surface and topography effects, radiative transfer error uncertainty, snow vertical inhomogeneity and snow pollution, to name a few). The uncertainty in the derived atmospheric optical thickness (AOT) is expected to be (0.05+0.2*AOT) (Kaufman et al., 1997) for dark surfaces. The impact of this uncertainty on surface reflectance retrieval at the band used for the grain size retrieval (MODIS Band 5) can lead to typical absolute errors around 0.007 for AOT(0.55 μm)=0.1 and 0.016 for AOT(.55)=0.5. The correction for aerosol effects is based on AOT climatology when MODIS AOT product is not available to generate the Surface Reflectance MODIS product. Accuracy can deteriorate when this default AOT value departs from the actual one. Moreover, current MODIS aerosol retrieval algorithm is not capable to retrieve AOT over snow and only nearby dark pixels (e.g., water, bare soil, and rocks) should be used for the retrieval.

The choice of the aerosol model can cause uncertainty in the atmospheric correction. In example, for AOT(0.55 μm)=0.3 and sun zenith angle of 30° the absolute error estimated for band 5 is 0.016. The assumption of Lambertian surface can deteriorate the accuracy with larger errors occurring in the backscattering direction and for shorter wavelengths (bands 1, 3, and 4). Also calibration uncertainty can lead to relative and absolute errors at band 5 not greater than, respectively, 2% and 0.015 (http://modis-sr.ltdri.org/html/prodacc.htm). Other sources of error are due to shadows caused by clouds and topographic effects (Vermote & Vermeulen, 1999).

In order to study the impact of the uncertainty and accuracy of the MODIS product on the retrieval of grain size values we compute (by means of the equations of the model reported in Section 3) the values of the reflectance at three different wavelengths (1.1, 1.245 and 1.4 μm) for different values of grain size (called reference grain size). Then, we consider a variation of ±10% and ±5% on the value of the reflectance obtained with the values of reference grain size (reference reflectance) and compute the values of grain size matching the new values of the modified reflectance (matching grain size). The results are

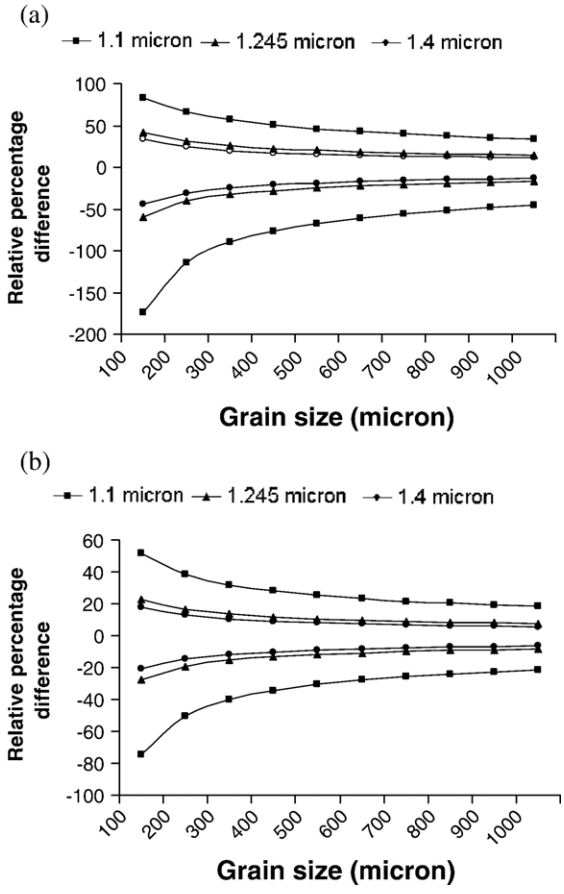

Fig. 11. Relative percentage difference between a reference grain size value (x-axis) and the value of grain size required for a change of 10% (a) or 5% (b) on the reference reflectance at the three different wavelengths of 1.1, 1.245 and 1.4 μm. Note that the scales on the y-axis of (a) and (b) are different.

displayed in Fig. 11. Here, on the *x*-axis we report the values of reference grain size where on the *y*-axis we report the relative percentage difference between the reference and matching values of grain size when the reference reflectance changes by ±10% (a) or ±5% (b). We observe that the relative percentage difference between the values of the reference and matching grain size decreases as the reference grain size and wavelength increase. Let us report a numerical example: if the reference value is 200 μm, then the values of the matching grain size can range within [174 μm–228 μm] at 1.4 μm, [167 μm–237 μm] at 1.245 μm and [123 μm–300 μm] at 1.1 μm in case of a ±5% variation of reference reflectance and within [151 μm–261 μm] at 1.4 μm, [138 μm–281 μm] at 1.245 μm and [67 μm–428 μm] at 1.1 μm in case of a ±10% variation of the reference reflectance value. The results displayed in Fig. 11 show that for low values of grain size the difference between the reference and matching values of grain size can be substantial, meaning that the effect of the uncertainty and error related to the MODIS product used for the retrieval play a fundamental role. Also, even for increasing dimension of grain size, the relative percentage difference can still be around ±20% (±35%) for a variation of ±5% (±10%) of the reference reflectance.

Another source of uncertainty that must be considered when comparing measured and retrieved values of grain size is the different resolution of the two data sets. Ground-based measurements are collected at point scale where satellite data here used have a resolution of 500 m. It must be said that each satellite pixel was including only one location of ground measurements and hence we are assuming that the value measured at point scale is representative of the 500 m × 500 m area. Besides, some satellite pixels were only partially covered by snow and this was not taken into account in our retrieval algorithm. The MODIS algorithm classifies as snow-covered pixels those ones where the Normalized Difference Snow Index (NDSI = (band 4 − band 6) / (band 4 + band 6)) is higher than 0.4, with band 6 corresponding to 1628–1652 nm and band 4 to 545–565 nm (Hall et al., 2001). Pixels having a NDSI smaller than 0.4 (snow cover percentage smaller than 50%) might still be classified as covered by snow after further analysis. During CLPX-1, high resolution data were acquired from satellite (Hyperion) and the Airborne Visible/Infrared Imaging Spectrometer (AVIRIS) which might be useful to quantify the snow cover percentage within each of the MODIS pixels. This is part of the planned future work.

7. Summary and conclusions

Grain size is a fundamental parameter of the snowpack, characterizing its thermodynamic state and controlling the spectral snow albedo. In the visible wavelengths, the sensitivity to grain size is small. But in the near-infrared band the reflectance shows a stronger sensitivity to the grain size than in the visible band, therefore making it possible to retrieve grain size at these wavelengths. We applied the asymptotic radiative transfer theory (Kokhanovsky & Zege, 2004) developed under the assumptions of fractal particles for retrieving the dimension of snow grains from near-infrared measurements of reflectance. Differently from most of the models currently used, which assume a spherical particle for grains, our model makes use of a fractal-based approach, where the particle is modeled as a Koch fractal of the second generation. We compared the spherical albedo obtained from ART in both cases of spherical and fractal particles and observed that the difference between the two hypotheses on the shape of the ice particles is significant in the near IR. The differences are smaller in the visible region. It is our recommendation that future studies will have to consider this aspect when comparing retrieved and measured values of grain size.

We tested SARA by using data collected during a ground-based controlled experiment. In this case the atmospheric effects were negligible and it was possible to compare the retrieved values with those obtained from observations and image processing analysis. We also compared the values retrieved by SARA with those obtained from a different algorithm. Results show us that SARA provided values of grain size close to that reported by Aoki et al. (2000) when using a spherical model in which only exact numerical calculations according to the radiative transfer theory were used. This suggests the general applicability of SARA. The results for the model in the case of fractal particles were found to be close to the values of grain size obtained with image processing (d_{image}). The reason for this is not clear because the meaning of the effective grain size and d_{image} are quite different. This aspect will be object of future investigation. However, we would like to point out here that the measurement of EGS using ground-based *in situ* techniques is a complex task and, therefore, the validation of the results presented here is not an easy matter. One way out of the problem might be the investigation of the possibility to correlate remotely sensed EGS with one or more parameters of grains easily measured using digital optical sizing techniques (e.g., the maximal size of grains d_{max}). Then it would be necessary to establish the proportionality constant $C = d/d_{\mathrm{max}}$ from correspondent experimental investigations. In conclusion, we underline that the validation of the retrieved EGS is one of main tasks of the further work.

The retrieval algorithm was applied to space-borne data measured by the Moderate Resolution Imaging Spectroradiometer (MODIS) to generate maps of grain size. The test area was located in Colorado and was one of the observation areas of the NASA Cold Land Processes Experiment-1 (CLPX-1). Within this framework, intensive measurements of grain size were carried out at several locations within an area of 25 km × 25 km. Unfortunately, because of cloudy sky conditions, it was not possible to perform a concurrent comparison between the values of grain size retrieved from MODIS data and those collected on ground. Hence, we were only able to compare the values of measured grain size with those derived from MODIS data acquired one or two days before. Results suggest that the algorithm applied to MODIS data is able to provide results consistent with those measured on the ground. Also, the values of grain size retrieved from morning and afternoon passes on February 19, 2003 show that the proposed technique is capable of detecting new snow , because of the small grain size. This aspect might be useful for detecting the presence of new snow on top of the old one for supporting avalanche modeling or forecasting. Also, this aspect

might be helpful for refining existing algorithms for the detection of frozen precipitation.

However many aspects have still to be investigated and resolved before the retrieval from space can be performed with high accuracy. Among these aspects we identified two of them: first, when comparing satellite retrieved and ground-measured values it is necessary to consider that the first are representative of an area where the second ones are collected at local scale and having more measurements within a single satellite pixel would help to compare retrieved and measured values. Second, the sensitivity of the retrieval to the error introduced by atmospheric correction can be substantial. In example, for values of grain size of 200 μm an error of ±5% (10%) on the estimation of the reflectance can lead to an error of ±20% (±40%) on the estimation of grain size. For larger grain size, the relative percentage difference can still be around ±20% (±35%) for a variation of ±5% (±10%) of the reference reflectance.

Acknowledgments

The authors would like to acknowledge Teruo Aoki for providing the ground based data used in this study and Eleonora Zege for a number of important advices on the initial stage of this work.

References

Aoki, T., Fukabori, M., Hachikubo, A., Tachibana, Y., & Nishio, F. (2000). Effects of snow physical parameters on spectral albedo and bidirectional reflectance of snow surface. *Journal of Geophysical Research*, *105*(D8), 10219−10236.

Aoki, T., Hori, M., Motoyoshi, H., Tanikawa, T., Hachikubo, A., Sugiura, K., et al. (2005). Validation results of ADEOS-II/GLI snow products. *Proceedings of IGARSS 2005, Seoul, Korea*.

Bourdelles, B., & Fily, M. (1993). Snow grain-size determination from Landsat imagery over Terre Adelie, Antarctica. *Annals of Glaciology*, *17*, 86−92.

Dominé, F., Salvatori, R., Legagneux, L., Salzano, R., Fily, M., & Cassachia, R. (2006). Correlation between the specific surface area and the short wave infrared (SWIR) reflectance of snow. *Cold Regions Science and Technology*, *46*, 60−68.

Dozier, J., & Marks, D. (1987). Snow mapping and classification from Landsat Thematic Mapper data. *Annals of Glaciology*, *9*, 97−103.

Dozier, J., Schneider, S. R., & McGinnis, D. F., Jr. (1981). Effect of grain size and snowpack water equivalence on visible and near-infrared satellite observations of snow. *Water Resources Research*, *17*(4), 1213−1221.

Fily, M., Bourdelles, B., Dedieu, J. P., & Sergent, C. (1997). Comparison of *in situ* and Landsat Thematic Mapper derived snow grain characteristics in the Alps. *Remote Sensing of Environment*, *59*, 452−460.

Green, R. O., Dozier, J., Roberts, D. A., & Painter, T. H. (2002). Spectral snow reflectance models for grain size and liquid water fraction in melting snow for the solar reflected spectrum. *Annals of Glaciology*, *34*, 71−73.

Grenfell, T. C., Neshyba, S. P., & Warren, S. G. (2005). Representation of a nonspherical ice particle by a collection of independent spheres for scattering and absorption of radiation: 3. Hollow columns and plates. *Journal of Geophysical Research (Atmospheres)*, *110*, D17203.

Grenfell, T. C., & Warren, S. G. (1999). Representation of a nonspherical ice particle by a collection of independent sphere for scattering and absorption of radiation. *Journal of Geophysical Research*, *104*, 31,697−31,709.

Hall, D. K., Riggs, G. A., & Salomonson, V. (2001). Algorithm Theoretical Basis Document (ATBD) for the MODIS Snow and Sea Ice-Mapping Algorithms available at http://modis.gsfc.nasa.gov/data/atbd/atbd_mod10.pdf

Hansen, J. E., & Travis, L. D. (1974). Light scattering in planetary atmospheres. *Space Science Reviews*, *16*, 527−610.

Kokhanovsky, A. A. (2005). Reflection of light from a semi-infinite medium with irregularly shaped particles. *Journal of Quantitative Spectroscopy & Radiative Transfer*, *96*, 1−10.

Kokhanovsky, A. A. (2006). Cloud Optics Berlin: Springer.

Kokhanovsky, A. A., Aoki, T., Hachikubo, A., Hori, M., & Zege, E. P. (2005). Reflective properties of natural snow: approximate asymptotic theory versus *in situ* measurements. *IEEE Transactions on Geoscience and Remote Sensing*, *43*(7), 1529−1538.

Kokhanovsky, A. A., & Nauss, T. (2006). Reflection and transmission of solar light by clouds: Asymptotic theory. *Atmospheric Chemistry and Physics*, *6*, 5537−5545.

Kokhanovsky, A., Rozanov, V. V., Zege, E. P., Bovensmann, H., & Burrows, J. P. (2003). A semi-analytical cloud retrieval algorithm using backscat-tering radiation in 04.–2.4 μm spectral range. *Journal of Geophysical Research D*, *108*. doi:10.1029/2001JD001543

Kokhanovsky, A., & Zege, E. P. (2004). Scattering optics of snow. *Applied Optics*, *43*, 1589−1602.

Kaufman, Y. J., Kleidman, R. G., Hall, D. K., Martins, J. V., & Barton, J. S. (2002). Remote sensing of subpixel snow cover using 0.66 and 2.1 μm channels. *Geophysical Research Letters*, *29*(16). doi:10.1029/2001GL013580

Kaufman, Y. J., Tanré, D., Remer, L., Vermote, E. F., Chu, A., & Holben, B. N. (1997). Operational remote sensing of tropospheric aerosol over the land from EOS-MODIS. *Journal of Geophysical Research*, *102*(14), 17051−17068.

Legagneux, L., Cabanes, A., & Dominé, F. (2002). Measurement of the specific surface Area of 176 snow samples using methane adsorption at 77 K. *Journal of Geophysical Research*, *107*, 4335. doi:10.1029/2001JD001016

Li, W., Stamnes, K., & Chen, B. (2001). Snow grain size retrieved from near-infrared radiances at multiple wavelengths. *Geophysical Research Letters*, *28*(9), 1699−1702.

Macke, A., Mueller, J., & Raschke, E. (1996). Scattering properties of atmospheric ice crystals. *Journal of the Atmospheric Sciences*, *53*, 2813−2825.

Mie, G. (1908). Bitrage zur Optik truber Medien speziell kolloidaler Metallosungen. *Annalen der Physik*, *25*, 377−445.

Neshyba, S. P., Grenfell, T. C., & Warren, S. G. (2003). Representation of a nonspherical ice particle by a collection of independent spheres for scattering and absorption of radiation. *Journal of Geophysical Research*, *108*(D15).

Nolin, A. W., & Dozier, J. (1993). Estimating snow grain size using AVIRIS data. *Remote Sensing of Environment*, *44*, 231−238.

Nolin, A. W., & Dozier, J. (2000). A hyperspectral method for remotely sensing the grain size of snow. *Remote Sensing of Environment*, *74*(2), 207−216.

Painter, T. H., & Dozier, J. (2004). Measurements of the hemispherical-directional reflectance of snow at fine spectral and angular resolution. *Journal of Geophysical Research (Atmospheres)*, *109*, D18.

Painter, T. H., Dozier, J., Roberts, D. A., Davis, R. E., & Greene, R. O. (2003). Retrieval of subpixel snow-covered area and grain size from imaging spectrometer data. *Remote Sensing of Environment*, *85*, 64−77.

Riggs, G. (2006), Pers. Comm.

Tanikawa, T., Aoki, T., & Nishio, F. (2002). Remote sensing of snow grain-size and impurities from Airborne Multispectral Scanner data using a snow bidirectional reflectance distribution function model. *Annals of Glaciology*, *34*, 74−80.

Van de Hulst, H. C. (1980). Multiple light scattering N.Y.: Academic Press.

Vermote, E., & Vermeulen, A. (1999). Atmospheric correction algorithm: Spectral reflectances (MOD09), ATBD version 4.0 available at http://eospso.gsfc.nasa.gov/ftp_ATBD/REVIEW/MODIS/ATBD-MOD-08/atbd-mod-08.pdf

Wiscombe, W., & Warren, S. (1980). A model for the spectral albedo of snow I. Pure snow. *Journal of the Atmospheric Sciences*, *37*, 2712−2733.

Wiscombe, W., & Warren, S. (1980). A model for the spectral albedo of snow II. Snow containing atmospheric aerosols. *Journal of the Atmospheric Sciences*, *37*, 2734−2745.